METTL14 Suppresses Pyroptosis and Diabetic Cardiomyopathy by Down-Regulating TINCR lncRNA

Liping Meng
Shaoxing Hospital of Zhejiang University
Hui Lin
Shaoxing Hospital of Zhejiang University
Xingxiao Huang
Shaoxing Hospital of Zhejiang University
Jingfan Wen
Shaoxing Hospital of Zhejiang University
Shengjie Wu (wusj120@163.com)
The First Affiliated Hospital of Wenzhou Medical University

Original investigation

Keywords: Diabetic cardiomyopathy, METTL14, LncRNA, pyroptosis, NLRP3

Posted Date: June 24th, 2021

DOI: https://doi.org/10.21203/rs.3.rs-642694/v1

Abstract

Background: N6-methyladenosine (m6A) is one of the most important epigenetic regulation of RNAs, such as lncRNAs. However, the underlying regulatory mechanism of m6A in diabetic cardiomyopathy (DCM) is very limited. In this study, we sought to define the role of METTL14-mediated m6A modification in pyroptosis and DCM progression.

Methods: DCM rat model was established and qRT-PCR, western blot and immunohistochemistry (IHC) were used to detect the expression of METTL14 and TINCR. Gain-and-loss functional experiments were performed to define the role of METTL14-TINCR-NLRP3 axis in pyroptosis and DCM. RNA pulldown and RNA immunoprecipitation (RIP) assays were carried out to verify the underlying interaction.

Results: In vivo and in vitro studies showed that pyroptosis was tightly involved in DCM progression. METTL14 was downregulated in cardiomyocytes and hear tissues of DCM rat tissues. Functionally, METTL14 suppressed pyroptosis and DCM via downregulating lncRNA TINCR, which further decreased the expression of key pyroptosis-related protein, NLRP3. Mechanistically, METTL14 increased m6A methylation level of TINCR gene, resulting in its downregulation. Moreover, the m6A reader protein YTHDF2 was essential for m6A methylation and mediated the degradation of TINCR. Finally, TINCR positively regulated NLRP3 through increasing its mRNA stability.

Conclusions: Our work revealed the novel role of METTL14-mediated m6A methylation and lncRNA regulation in pyroptosis and DCM, which could help extend our understanding the epigenetic regulation of pyroptosis in DCM progression.

Introduction

Diabetic cardiomyopathy (DCM), a major cardiovascular complication of diabetes, is characterized by myocardial fibrosis, ventricular remodeling, and cardiac dysfunction (1). DCM is closely associated with occurrence of heart failure, making it the majority cause of death among patients with diabetes (2). DCM influence heart healthy through various mechanisms, including changes of metabolism, abnormal subcellular composition, and damage of microvascular (3). However, the detailed mechanism of DCM is not well known and remains elusive. Revealing the key genes involved in DCM and identifying the potential regulatory mechanism will provide therapeutic targets used for overcoming DCM.

Pyroptosis is characterized by rapid plasma membrane rupture, with the consequent release of intracellular contents and pro-inflammatory mediators, such as caspase-1 (4). The main signaling pathway involved in pyroptosis is mediated by caspase-1 activation, resulting in the maturation process of IL-1β, IL-18 and gasdermin D (GSDMD) (5). Previous studies widely reported the essential role of pyroptosis in cardiomyopathy, especially in DCM (6). Xie et al. demonstrated that NLRP3 inflammasome mediated the chemerin/CMLR1-induced inflammation and pyroptosis and contribute to DCM (7). Another research by Cao et al. revealed that high glucose induced cardiotoxicity by inhibiting NLRP3 inflammasome activation and pyroptosis (8).

As the most abundant chemical modification of eukaryotic messenger RNA (mRNA), N6-methyladenosine (m6A) is known to influence various fundamental bioprocesses by regulating target gene expression (9). m6A regulatory proteins are composed of the “erasers” FTO and ALKBH5, the “readers” YTHDFs and IGF2BPs, and the “writers” METTL3, METTL14 and WTAP (10). Alterations in the m6A level mediate cell apoptosis, proliferation, self-renewal and development (11). However, the potential role of m6A methylation in DCM progression remains unknown.

Methyltransferase-like 14 (METTL14), a well-known m6A writer protein, widely participated in the progression of major diseases, such as cardiovascular pathogenesis (12). However, whether METTL14 regulates DCM and the underlying mechanism are under investigation. In this study, we revealed that METTL14 was downregulated in myocardium tissues of DCM rat, and high glucose suppressed the METTL14 expression level. Mechanistically, the METTL14-mediated activity of m6A modification of TINCR suppressed pyroptosis of cardiomyocytes and DCM in an NLRP3-dependent manner.

Materials And Methods

Cell lines and chemical reagent

As we previously described (13), primary neonatal rat cardiomyocytes (PNRC) were obtained from isolated heart tissues of young Wistar rats. Briefly, the dissected hearts minced in HEPES-buffered nic acid saline solution. Non-myocyte contaminants were removed by two rounds of pre-plating for 1.5 h on 100-mm plastic cell culture dishes under a culture condition of 37 °C and 5% CO_2. Then, the cardiomyocytes were seeded into different culture dishes with medium containing serum. After incubation for 24 hours, medium without serum was used to replace the serum-containing medium.

The normal H9c2 cardiomyocyte cell line was purchased from American Type Culture Collection (ATCC). Cells were cultured with 1640 medium containing 10% fetal bovine serum in a humidified atmosphere of 5% CO_2 at 37°C. Actinomycin D was purchased from Sigma-Aldrich and used at the concentration of 5 μg/ml. MCC950 sodium (CP-456773, CRID3 sodium salt), a NLRP3 inhibitor, was used at the concentration of 7.0 nM in cell culture and 12 mg/kg in animal treatment (Selleck, Shanghai, China).

Establishment and treatment of diabetic animal models

Male Sprague-Dawley rats weighing 200-250 g were purchased from Model Animal Research Center of Nanjing University. The diabetic model was constructed by a single intraperitoneal injection of streptozotocin (65 mg/kg). The fasting blood glucose was measured one week after injection. Only rats with glucose levels higher than 16.7 mmol/L were defined as diabetic. Cardiac function was investigated 7 days following the last treatment, and the heart tissues were then isolated for expression analyses. The lentivirus vector used for silencing or overexpressing specific genes were dissolved in 50 μL saline at the concentration of 1×10^9 TU.

RNA extraction and quantitative RT-PCR

Total RNA was isolated by TRIzol reagent (Invitrogen, Carlsbad, CA). A total of 1 mg of extracted RNA was used to perform reverse transcription using Superscript III transcriptase (Invitrogen). Quantitative real-time PCR (qRT-PCR) was performed using SYBR Green real-time PCR analysis using Bio-Rad CFX96 system (Bio-Rad, Cambridge, MA) with the specific primers. Expression of the PCR data were shown as $2^{-\Delta\Delta ct}$, and normalized to the internal control level (GAPDH).

Echocardiography

Echocardiography was performed using a Vivid 7 Dimension (GE Healthcare, Munich, Germany) echocardiograph equipped with a 14-MHz transducer. Parasternal short-axis views were used for M-mode analysis. Enddiastolic and endsystolic left ventricular inner diameters (LVIDd, LVIDs) were measured and fractional shortening (FS) and left ventricular ejection fraction (LVEF) were calculated using the following equations: FS=(LVIDd-LVIDs)/LVID, LVEF=($LVIDd^3$-$LVIDs^3$)/$LVIDd^3$.

Transmission electron microscopy

Hearts were extracted, cut finely into small (~1 mm^3) blocks and fixed overnight in 4% glutaraldehyde in 100 mM phosphate buffer, followed by post-fixation in 2% osmium tetroxide in 100 mM phosphate buffer. Specimens then underwent en bloc treatment with uranyl acetate, dehydration in ethanol, and transferred to propylene oxide, prior to embedding. Ultra-thin sections (50-70 nm) were cut and stained with uranyl acetate and lead citrate, and examined in a JEOL 1200EX electron microscope.

TUNEL assay

Cells were firstly fixed with 4% paraformaldehyde for 30 min followed by staining with one-step TUNEL kit as per the instructions of manufacture (Beyotime, Shanghai, China). The positive stained parts were visualized and calculated via a fluorescence microscopy (Axio Observer A1, ZEISS, Germany).

IHC analysis

Heart myocardial tissues were isolated and fixed with 4% Paraformaldehyde following with incubation with primary antibodies against respective proteins: NRLP3 (1:100, cat. no. ab214185, Abcam, Cambridge, MA), METTL14 (1:100, ab223090, Abcam), cleaved caspase-1 (1:100, ab1872, Abcam), IL-1β (1:100, ab2105, Abcam) and IL-18 (1:100, ab18672, Abcam), to detect their expression levels. Images were visualized using a ZEISS Axio Observer A1 (Oberkochen, Germany) microscope system and processed with ZEISS software.

RIP and RNA pulldown assay

The RNA immunoprecipitation (RIP) was performed using the EZ-Magna RIP kit (Millipore, Burlington, MA, USA) according to the manufacturer's instructions. Briefly, 10^7 cells were lysed with RIP lysis buffer using one freeze-thaw cycle. Cell extracts were coimmunoprecipitated with anti-m6A (ab208577, Abcam) and NLRP3 (ab263899, Abcam) antibodies and the retrieved RNA was subjected to qRT-PCR analysis.

The RNA pulldown assay was performed using a Magnetic RNA-Protein Pull-down Kit (Thermo Scientific) according to manufacturer's instructions. The 3'-end Biotin-TEG modified-DNA probes against TINCR were synthesized by Sangon (Shanghai, China). The cell lysates were hybridized with a mixture of biotinylated DNA probes for 4 h at 37 °C. The binding complexes were then recovered using streptavidin-conjugated magnetic beads. Finally, protein was eluted and purified from the beads for western blot analyses.

Western blots

Protein extraction were performed using RIPA lysis buffer (Pierce, IL, USA) containing protease inhibitor (Roche, CA, USA). Protein extracts were subjected to 10% SDS-polyacrylamide gel electrophoresis followed by electro-transfer to polyvinylidene difluoride membrane. After 1h of pre-membrane blocking with 5% BSA, the proteins were incubated with respective primary antibodies at 4°C overnight followed by secondary antibodies incubation at room temperature for 1 h. The detection of proteins was carried out using ECL reagent.

Statistical analysis

All experiments were performed in triplicate. Statistics were presented as mean ± SD. Comparison between two groups were analyzed using the Student's t-test. Fisher exact testing was performed to evaluate the difference of proportions between different groups. Statistical analyses were performed using GraphPad Prism (v8.0.1, GraphPad Software Inc., San Diego, CA, USA). $P<0.05$ was considered to indicate a statistically significant difference.

Results

Pyroptosis is involved in DCM through NLRP3-caspase-1 pathway in vitro

We treated neonatal rat cardiomyocytes (PNRC) and cardiomyocyte cell line H9c2 with glucose at the concentration of 5.5 mmol/L (normal control) or 50 mmol/L (high glucose, HG) to imitate the hyperglycemic condition. As shown in Figure 1A, due to the HG treatment, H9c2 cells exhibited characteristic morphological changes, such as swelling changes and rupture of cell membrane, suggesting that pyroptosis was directly involved in DCM process. Then we performed Calcein-AM staining analysis and found that HG treatment caused an increased damage of cell membrane when compared with control treatment (Figure 1B). Moreover, the protein expression of pyroptosis markers, including NLRP3, cleaved caspase-1, and GSDMD-N, were significantly upregulated in HG-

treated cardiomyocytes (Figure 1C). Importantly, treatment with MCC950, a well-known NLRP3 inhibitor, dramatically reversed pyroptosis of cells treated with HG (Figure 1C). We also evaluated the effect of HG treatment on cell apoptosis by performing TUNEL staining. As shown, apoptosis was activated by upon HG treatment, however, this activation was not restored by MCC treatment (Figure 1D). These data showed that HG treatment resulted in pyroptosis of cardiomyocytes in an NLRP3-dependent manner.

Pyroptosis was activated in cardiomyocyte of DCM rats

To further verify the essential role of pyroptosis in HG-induced toxicity of cardiomyocytes, we constructed DCM model using Wistar rats by single intraperitoneal injection of streptozotocin. Echocardiography was performed to evaluate the cardiac function of DCM rats. Our data revealed a reduced LVEF and FS in rats with DCM in contrast to normal rats. The LVEF level of DCM rats was 48%, which is significantly lower than that in normal rats (68%). Moreover, the average FS of rats with DCM was also dramatically decreased compared to control rats (21% vs. 37%) (Figure 2A). Interestingly, when NLRP3 was silenced with MCC950 in DCM rats, the damaged cardiac function caused by DCM was dramatically reversed (Figure 2A). By detecting myocardial enzyme markers, such as AST, LDH and CK-MB, we identified an elevated expression in DCM rats, however, MCC950 treatment partly restored this effect. (Figure 2B). In addition, electron microscopy imaging of cardiomyocyte ultrastructure showed that DCM rats showed serious cardiomyocyte damage compared to control hearts, including increased inter-mitochondrial distance, disconnected cardiac myofibers and thinner myofibers, and this damage could be partially rescued by MCC950 (Figure 2C). Finally, the expressions of pyroptosis proteins, NLRP3 and GSDMD-N, were dramatically increased in rats of DCM compared, meanwhile, this influence was significantly relieved by MCC950 (Figure 2D). Finally, the pyroptosis in DCM was finally proved by Masson staining (Figure 2E). Taken together, we demonstrated that DCM was closely associated with cardiomyocytes pyroptosis in an NLRP3-dependent manner.

METTL14 is downregulated in DCM

To find whether METTL14 was involved in pyroptosis in DCM models, we detected the expression level of METTL14 in DCM rats. As shown in Figure 3A-B, METTL14 was significantly downregulated in heart tissue and serum samples of DCM rats compared to those of controlled rats. Moreover, a decreased METTL14 level was identified in PNRC and H9c2 cells treated with HG when compared with control cells (Figure 3C-D). In addition, serum METTL14 was also downregulated in patients with DCM than that of healthy individuals (Figure 3E). These results indicate that METTL14 may be key molecular regulator during DCM initiation and progression.

METTL14 suppresses DCM via modulating pyroptosis

To clarify the role of m6A modification in pyroptosis and DCM progression, we evaluated the effect of METTL14 in DCM progression. As expected, injection of Lv-METTL14 into DCM rats significantly increased m6A level in DCM rats (Figure 4A-B). Echocardiography suggested that overexpression of METTL14 increased LVEF, FS (Figure 4C). Meanwhile, electron microscopy revealed a relieved injury in cardiomyocyte (Figure 4D). Moreover, enhanced METTL14 inhibited pyroptosis level in myocardial tissues, including downregulation of NLRP3, caspase-1 and GSDMD-N (Figure 4E), suggesting that METTL14-mediated m6A modification may suppress DCM through modulating pyroptosis. To confirm this hypothesis in vitro, we silenced METTL14 and m6A modification level in H9c2 and PNRC cells (Figure 4F-G). Reversed morphologic changes of pyroptosis were observed upon silence of METTL14 (Figure 4H). Western blotting showed that sh-METTL14 caused upregulated NLRP3, cleaved caspase-1 and GSDMD-N (Figure 4I). Consistently, Calcein-AM staining revealed an increased membrane damage in H9c2 cells silenced with METTL14 compared to controls, however, this effect was abrogated by MCC950 (Figure 4J). Collectively, we proved that METTL14-mediated m6A modification play essential roles in DCM via regulating cardiomyocyte pyroptosis.

METTL14 suppresses pyroptosis via targeting TINCR lncRNA

It is reported that m6A process was closely associated with lncRNA processing (14). By performing GSEA analysis, we revealed that METTL14 was involved in the process and degradation of ncRNAs (Figure 5A). Based on our previous observation of lncRNA TINCR in pyroptosis, we supposed that METTL14 may regulate DCM through TINCR-mediated pyroptosis. To prove this assumption, we detected TINCR expression and found that TINCR was negatively correlated with METTL14 in patients with DCM (Figure 5B). In addition, TINCR was upregulated in HG-treated cells and DCM rats (Figure 5C-D). Next, we silenced METTL14 in PNRC and H9c2 cells, and found that TINCR was upregulated accordingly (Figure 5E), while overexpression of METTL14 leads to a decreased expression of TINCR (Figure 5F).

Then, we performed gain-or-loss functional assays by injection TINCR lentiviral vector into METTL14-overexpressing DCM rats. Intriguingly, overexpression of TINCR reversed the METTL14-induced effects on LVEF, FS, and cardiomyocyte damage in DCM rats (Figure 5G-H). In addition, enhanced TINCR abrogated METTL14-caused suppression of pyroptosis in PNRC and H9c2 cells (Figure 5I). Collectively, we proved that lncRNA TINCR was, at least partly, responsible for METTL14-induced suppression of pyroptosis and DCM.

METTL14-dependent m6A methylation downregulated expression of TINCR

Take a step further, we sought to find whether it is the METTL14-mediated m6A modification that downregulated TINCR expression. By analyzing the potential m6A binding sites with online SRAMP database (http://www.cuilab.cn/sramp), we verified 45 m6A residues located across TINCR sequence (Figure 6A), among which 11 were identified as *high/very high confidence* (Table 1). It is well demonstrated that METTL14 acted as an interactor with WTAP, binding to the methyltransferase to form a complex which mediates m6A methylation on RNAs. Here, sh-WATP vector was injected into METTL14-overexpressed DCM rats (Figure 6B). Suppressed TINCR caused by METTL14 was abrogated by silence of WATP (Figure 6C). Then, we performed RIP assay using m6A antibody, and found a significantly decreased methylated TINCR (site 7709) bounded by m6A upon METTL14 deletion or WTAP deletion (Figure 6D). Above results strongly suggest that METTL14-dependent m6A modification of TINCR results in its downregulation.

m6A methylation is a characterized process which needs the involvement of m6A reader proteins, including YTHDFs (15). Given that YTHDF2 participated in modulation of m6A-dependent RNA degradation (16), we therefore assumed that YTHDF2 may be essential for METTL14-mediated TINCR decay and downregulation. By performing RIP using antibody against YTHDF2, we identified the positive binding of TINCR by YTHDF2 antibody in DCM rats (Figure 6E). Consistently, RNA pulldown assay showed that YTHDF2 was significantly enriched by TINCR (Figure 6F). Then, we silenced YTHDF2 expression in cardiomyocytes (Figure 6G). The decay rate of TINCR was significantly slower in shYTHDF2-infected cells (Figure 6H), indicating that YTHDF2 mediated m6A-RNA decay of TINCR. Altogether, our results revealed that METTL14-mediated m6A modification inhibited TINCR expression via YTHDF2-regulated RNA degradation.

TINCR promotes pyroptosis and DCM via stabilizing NLRP3 mRNA

Previously, we demonstrated that TINCR regulated cardiomyocytes pyroptosis via stabilizing NRLP3 in DOX-induced cardiotoxicity (13). To verify whether this regulation mode applies in DCM, we performed gain-and-loss functional assays. As shown, MCC950 remarkedly abrogated the TINCR-regulated pyroptosis in HG-treated cardiomyocytes (Figure 7A). To further confirm the direct interaction between TINCR and NLRP3 RNA, we conducted RNA pulldown assay by generating biotinylated oligonucleotides in HG-treated H9c2 and PNRC cells. As shown, NLRP3 RNA was remarkably enriched by biotinylated TINCR (Figure 7B). By treatment with actinomycin D (ActD), a well-known inhibitor for RNA transcription, we evaluated the effect of TINCR on downstream mRNA degradation. The results revealed that knockdown of TINCR resulted in an accelerated degradation of NLRP3 mRNA in cardiomyocytes (Figure 7C). More importantly, METTL14 decreased the stability of NLRP3, and overexpression of TINCR reversed this effect (Figure 7D). Collectively, the above results which strongly supports that METTL14-mediated m6A induced suppression of TINCR, which further regulates pyroptosis via stabilizing NLRP3 mRNA (Figure 7E).

Discussion

It is estimated that DCM occurs in approximately 12% of diabetic patients (17). Clinical data suggests that DCM is closely associated with Clinical studies indicate that DCM increases the risk of overt heart failure and induces worse prognosis in diabetic patients (18). A strategy for prevention and treatment in order to improve the prognosis of DCM has not been established. In this study, we established that METTL14, a well-known m6A writer, inhibited pyroptosis and DCM through downregulation of lncRNA TINCR and NLRP3 expression. Mechanistically, METTL14 mediated m6A modification of TINCR, and thus suppressed TINCR expression and the NLRP3 stability, preventing the occurrence of pyroptosis.

DCM is characterized by structural and functional disorders, including myocardial cell death, myocardial fibroblast activation, left ventricular dysfunction, and metabolic deregulation (19). Pyroptosis is characterized with programmed cell death inflammation, and has been proved crucial for controlling microbial infections (20). Accumulating evidence suggests that pyroptosis may contribute to a range of diseases, including autoimmune diseases, diabetes mellitus, nervous system-related diseases and cardiovascular diseases (21–23). Several reports showed that pyroptosis was closely associated with DCM progression (24). Moreover, HG treatment could lead to the produce of active oxygen species, resulting in inflammation accompanied with elevated expression of cleaved caspase-1, IL-1β and IL-18 (25). In addition, the activation of the inflammasome and the release of cytokines can promote the deposition of collagens and fibrotic formation, further exacerbating the severity of DCM (26). Our study further confirmed that pyroptosis was involved in DCM both in vitro and in vivo. Moreover, this regulation mainly through the regulation of NLRP3 inflammasome.

The m6A modification is deposited to RNAs by the m6A methyltransferase (writer) complex, a protein complex formed by METTL3/METTL14 heterodimeric catalytic core and a regulatory subunit, WTAP. METTL3 and METTL14 are co-located in nuclear spots and form stable complexes in a 1:1 ratio (27). METTL14 is a pseudo-methyltransferase that stabilizes METTL3 and recognizes target RNA (28). Here is emerging evidence to indicate that m6A modification is closely related to the occurrence and progression of CVDs, including cardiac hypertrophy, heart failure, ischemic heart disease, etc. Dorn et al (10) demonstrated that METTL3-mediated m6A modification is significant for maintaining cardiac homeostasis and normal cardiac function and revealed increased m6A methylation in cardiomyocytes under hypertrophic stimulation. However, whether METTL14 is involved in cardiovascular diseases, such as DCM are largely unknown. Our study confirmed that METTL14 was downregulated in DCM models and remarkably suppressed DCM. More importantly, METTL14 inhibits pyroptosis in a NLRP3-dependent manner, which uncovered a novel functional role of METTL14 in pyroptosis and pyroptosis-induced DCM.

Recent studies have found that, in addition to the roles of m6A modifications in mRNAs, m6A modifications regulate the generation and function of noncoding RNAs, such as lncRNAs. LncRNAs are a class of transcripts more than 200 nucleotides long with no protein-coding function (29). m6A modifications might modulate the function of lncRNAs by providing a binding site for the m6A reader proteins or by modulating the structure of the local RNA to induce RNA-binding protein entry. Previous study showed that knocking down METTL3 reduced the level of m6A modifications on specific transcripts such that the lncRNA X chromosome was inactivated (30). Gone et al. demonstrated that METTL14 mediated m6A modification suppressed LncRNA ZFAS1/ RAB22A expression and provided novel therapeutic targets for atherosclerosis (31). Many lncRNAs show temporal differential expression, and display genic distribution in the genome. Interestingly, temporal-specific m6A-methylation with consensus m6A motif GGACU was reported in the last exon in most lncRNAs, indicating the potential way of interaction between m6A-methylation and lncRNA expression (32). Our former study revealed the essential role of lncRNA TINCR in pyroptosis and myocardial damage. With the consistent functions between METTL14 and TINCR, we investigated the potential regulatory mode of METTL14 and TINCR. By predicting with an online software, we uncovered several potential binding sites of m6A. RIP assay further confirmed the direct interaction.

The current hypothesis suggests that for m6A modification to exert its biological functions, it must first be recognized by m6A reader proteins. Human YTH domain family proteins include three members, YTHDF1-3, each of which comprise a highly conserved single-stranded RNA-binding domain located at the carboxy terminus (the YTH domain) and a less conserved amino-terminal region (33). The fates of m6A modified mRNAs are dependent on m6A selective binding proteins (34). YTHDF2 is the first identified and well-studied functional m6A-binding protein that mainly regulates stability of mRNA (35). YTHDF2 recognizes and binds to m6A sites in 3'UTR of mRNA through its C-terminal YTH domain to accelerate degradation of target mRNAs (36). As METTL14

decreased the expression of TINCR, we supposed the m6A reader could be YTHDF2 and finally, this hypothesis was confirmed, which further strengthen our previous report.

The regulation of NLRP3-based pyroptosis by TINCR has been well defined in DOX-induced myocardial damage in our previous study. Importantly, the regulation mode also applies to DCM. This commonly used pathway in pyroptosis suggests a tight correlation between TINCR-NLRP3 pathway and pyroptosis regardless of the causes of pyroptosis. However, the detailed mechanism by which DCM/HG induced higher expression of TINCR is not well known, which is the limitation of this study. We will follow this study and continue exploring the underlying pathways.

In conclusion, we demonstrated that METTL14 suppresses pyroptosis and DCM progression via m6A methylation of TINCR mRNA in an NLRP3-dependent manner. Our study not only help better understanding the regulatory mechanism of METTL14-mediated m6A modification in myocardial damage, but also useful for finding promising drug targets and developing novel therapeutic strategies to overcome DCM.

Declarations

Ethics approval and Consent for publication

The study protocol was approved by the Research Ethics Committee of Shaoxing People's Hospital. Written informed consent for publication was obtained from all participants.

Availability of data and materials

The analyzed data sets generated during the study are available from the corresponding author on reasonable request.

Competing interests

The authors report that there are no conflicts of interest.

Funding

This study is supported by the National Natural Science Foundation of China (No. 82000252, 81900345); the Basic Public Welfare Research Project of Zhejiang Province (LGF19H020002); Project From Health Department of Zhejiang Provincial (2021RC032); Medical and Health Science and Technology Plan Project of Shaoxing City (2020A13018, 2018C30021)

Authors' contributions

Dr. Liping Meng, Hui Lin, and Shengjie Wu mainly designed and did the research. Dr. Xingxiao Huang and Dr.Jingfan Weng collected and analyzed the data.

Acknowledgements

Not applicable.

References

1. Levelt E, Gulsin G, Neubauer S, McCann GP. MECHANISMS IN ENDOCRINOLOGY: Diabetic cardiomyopathy: pathophysiology and potential metabolic interventions state of the art review. Eur J Endocrinol. 2018;178(4):R127-R39.
2. Murtaza G, Virk HUH, Khalid M, Lavie CJ, Ventura H, Mukherjee D, et al. Diabetic cardiomyopathy - A comprehensive updated review. Prog Cardiovasc Dis. 2019;62(4):315–26.
3. Nirengi S, Peres Valgas da Silva C, Stanford KI. Disruption of energy utilization in diabetic cardiomyopathy; a mini review. Curr Opin Pharmacol. 2020;54:82–90.
4. Liu X, Zhang Z, Ruan J, Pan Y, Magupalli VG, Wu H, et al. Inflammasome-activated gasdermin D causes pyroptosis by forming membrane pores. Nature. 2016;535(7610):153–8.
5. Broz P. Immunology: Caspase target drives pyroptosis. Nature. 2015;526(7575):642–3.
6. Yang F, Li A, Qin Y, Che H, Wang Y, Lv J, et al. A Novel Circular RNA Mediates Pyroptosis of Diabetic Cardiomyopathy by Functioning as a Competing Endogenous RNA. Mol Ther Nucleic Acids. 2019;17:636–43.
7. Xie Y, Huang Y, Ling X, Qin H, Wang M, Luo B. Chemerin/CMKLR1 Axis Promotes Inflammation and Pyroptosis by Activating NLRP3 Inflammasome in Diabetic Cardiomyopathy Rat. Front Physiol. 2020;11:381.
8. Cao R, Fang D, Wang J, Yu Y, Ye H, Kang P, et al. ALDH2 Overexpression Alleviates High Glucose-Induced Cardiotoxicity by Inhibiting NLRP3 Inflammasome Activation. J Diabetes Res. 2019;2019:4857921.
9. Liu K, Gao Y, Gan K, Wu Y, Xu B, Zhang L, et al. Prognostic Roles of N6-Methyladenosine METTL3 in Different Cancers: A System Review and Meta-Analysis. Cancer Control. 2021;28:1073274821997455.
10. Qin Y, Li L, Luo E, Hou J, Yan G, Wang D, et al. Role of m6A RNA methylation in cardiovascular disease (Review). Int J Mol Med. 2020;46(6):1958–72.
11. Zhang C, Fu J, Zhou Y. A Review in Research Progress Concerning m6A Methylation and Immunoregulation. Front Immunol. 2019;10:922.

12. Zhang BY, Han L, Tang YF, Zhang GX, Fan XL, Zhang JJ, et al. METTL14 regulates M6A methylation-modified primary miR-19a to promote cardiovascular endothelial cell proliferation and invasion. Eur Rev Med Pharmacol Sci. 2020;24(12):7015–23.
13. Meng L, Lin H, Zhang J, Lin N, Sun Z, Gao F, et al. Doxorubicin induces cardiomyocyte pyroptosis via the TINCR-mediated posttranscriptional stabilization of NLR family pyrin domain containing 3. J Mol Cell Cardiol. 2019;136:15–26.
14. Liu H, Xu Y, Yao B, Sui T, Lai L, Li Z. A novel N6-methyladenosine (m6A)-dependent fate decision for the lncRNA THOR. Cell Death Dis. 2020;11(8):613.
15. Jin D, Guo J, Wu Y, Yang L, Wang X, Du J, et al. m(6)A demethylase ALKBH5 inhibits tumor growth and metastasis by reducing YTHDFs-mediated YAP expression and inhibiting miR-107/LATS2-mediated YAP activity in NSCLC. Mol Cancer. 2020;19(1):40.
16. Yang X, Zhang S, He C, Xue P, Zhang L, He Z, et al. METTL14 suppresses proliferation and metastasis of colorectal cancer by down-regulating oncogenic long non-coding RNA XIST. Mol Cancer. 2020;19(1):46.
17. Tarquini R, Pala L, Brancati S, Vannini G, De Cosmo S, Mazzoccoli G, et al. Clinical Approach to Diabetic Cardiomyopathy: A Review of Human Studies. Curr Med Chem. 2018;25(13):1510–24.
18. Shaher F, Qiu H, Wang S, Hu Y, Wang W, Zhang Y, et al. Associated Targets of the Antioxidant Cardioprotection of Ganoderma lucidum in Diabetic Cardiomyopathy by Using Open Targets Platform: A Systematic Review. Biomed Res Int. 2020;2020:7136075.
19. Adeghate E. Molecular and cellular basis of the aetiology and management of diabetic cardiomyopathy: a short review. Mol Cell Biochem. 2004;261(1–2):187–91.
20. Xia X, Wang X, Zheng Y, Jiang J, Hu J. What role does pyroptosis play in microbial infection? J Cell Physiol. 2019;234(6):7885–92.
21. Wan T, Li X, Li Y. The role of TRIM family proteins in autophagy, pyroptosis, and diabetes mellitus. Cell Biol Int. 2021.
22. Wu J, Sun J, Meng X. Pyroptosis by caspase-11 inflammasome-Gasdermin D pathway in autoimmune diseases. Pharmacol Res. 2021:105408.
23. McKenzie BA, Dixit VM, Power C. Fiery Cell Death: Pyroptosis in the Central Nervous System. Trends Neurosci. 2020;43(1):55–73.
24. Xu Y, Fang H, Xu Q, Xu C, Yang L, Huang C. LncRNA GAS5 inhibits NLRP3 inflammasome activation-mediated pyroptosis in diabetic cardiomyopathy by targeting miR-34b-3p/AHR. Cell Cycle. 2020;19(22):3054–65.
25. Gan J, Huang M, Lan G, Liu L, Xu F. High Glucose Induces the Loss of Retinal Pericytes Partly via NLRP3-Caspase-1-GSDMD-Mediated Pyroptosis. Biomed Res Int. 2020;2020:4510628.
26. Fuentes-Antras J, Ioan AM, Tunon J, Egido J, Lorenzo O. Activation of toll-like receptors and inflammasome complexes in the diabetic cardiomyopathy-associated inflammation. Int J Endocrinol. 2014;2014:847827.
27. Wang P, Doxtader KA, Nam Y. Structural Basis for Cooperative Function of Mettl3 and Mettl14 Methyltransferases. Mol Cell. 2016;63(2):306–17.
28. Weng H, Huang H, Wu H, Qin X, Zhao BS, Dong L, et al. METTL14 Inhibits Hematopoietic Stem/Progenitor Differentiation and Promotes Leukemogenesis via mRNA m(6)A Modification. Cell Stem Cell. 2018;22(2):191–205. e9.
29. Tao L, Yang L, Huang X, Hua F, Yang X. Reconstruction and Analysis of the lncRNA-miRNA-mRNA Network Based on Competitive Endogenous RNA Reveal Functional lncRNAs in Dilated Cardiomyopathy. Front Genet. 2019;10:1149.
30. Patil DP, Chen CK, Pickering BF, Chow A, Jackson C, Guttman M, et al. m(6)A RNA methylation promotes XIST-mediated transcriptional repression. Nature. 2016;537(7620):369–73.
31. Gong C, Fan Y, Liu J. METTL14 mediated m6A modification to LncRNA ZFAS1/ RAB22A: A novel therapeutic target for atherosclerosis. Int J Cardiol. 2021;328:177.
32. Nie Y, Tian GG, Zhang L, Lee T, Zhang Z, Li J, et al. Identifying cortical specific long noncoding RNAs modified by m(6)A RNA methylation in mouse brains. Epigenetics. 2020:1–17.
33. Zhang Z, Theler D, Kaminska KH, Hiller M, de la Grange P, Pudimat R, et al. The YTH domain is a novel RNA binding domain. J Biol Chem. 2010;285(19):14701–10.
34. Meyer KD, Jaffrey SR. Rethinking m(6)A Readers, Writers, and Erasers. Annu Rev Cell Dev Biol. 2017;33:319–42.
35. Wang X, Lu Z, Gomez A, Hon GC, Yue Y, Han D, et al. N6-methyladenosine-dependent regulation of messenger RNA stability. Nature. 2014;505(7481):117–20.
36. Zhu T, Roundtree IA, Wang P, Wang X, Wang L, Sun C, et al. Crystal structure of the YTH domain of YTHDF2 reveals mechanism for recognition of N6-methyladenosine. Cell Res. 2014;24(12):1493–6.

Tables

Table 1. verified 45 m6A residues located across TINCR sequence (Figure 6A), among which 11 were identified as *high/very high confidence*

TaRGET #	Position	Sequence context	Score(binary)	Score(knn)	Score(spectrum)	Score(coml
1	214	CCGCUGACCGUGCGGCCGCGGGACACGCUCAGCGACCUGCGCGCC	0.603	0.76	0.573	0.599
2	2054	GAAGGGCGCUGGGGCCACGGGAACAGCUCACUGCCGGCCUGGGGC	0.461	0.702	0.653	0.55
3	2169	ACCACCUCCUUGGAAGCAUUGAACAGGAGAGGGACGGGGGCCAUG	0.507	0.599	0.603	0.55
4	2494	UGGACGACCCUCAGACGUCCAGACUGUAAUUAUGCAGUACAGAGU	0.627	0.58	0.525	0.584
5	2548	UUGUGUGCCUACUGUGUGCCAGACUCCAUGCUGGACACUGAAAUU	0.49	0.473	0.61	0.537
6	2560	UGUGUGCCAGACUCCAUGCUGGACACUGAAAUUCAGCAGUGACCC	0.635	0.443	0.636	0.626
7	2820	UGUGCAAAGGCCCUGAGGCAGGACUGCACCUGGCAUGUUGGAGGA	0.717	0.691	0.325	0.559
8	2936	CAGUUCAUGCAGGGCCUUGCGGACUGCAGGGAGGACUUGGGCCUU	0.702	0.727	0.451	0.603
9	2948	GGCCUUGCGGACUGCAGGGAGGACUUGGGCCUUGACUCCGAGGGA	0.697	0.73	0.425	0.59
10	3060	CUGGCUGCAGCGGGGAGAACAGACUGUGAUGGGGGGAGGGCUGGA	0.752	0.747	0.543	0.668
11	3131	UGAGCCAUGCUGGAGGCAGAGAACAGAAGCCUUCAGAGGAGACAG	0.432	0.573	0.677	0.537
12	3150	AGAACAGAAGCCUUCAGAGGAGACAGUUUUGGCUGGGCGCAAUGG	0.474	0.423	0.637	0.536
13	3778	AGAAAUGAGAAAAACACUUGGGACCUGUCAGCGCAGACGGUACCC	0.588	0.629	0.577	0.586
14	3833	GAAGCUGCGUGGGCUGCUCGGGACAAACCUGCCAGGCCCUCUCUC	0.6	0.487	0.532	0.567
15	5987	UAGUAGUUGAGAAAGAGAAAGGACCUUAGAGAUUGUGGAGACCAU	0.623	0.711	0.483	0.572
16	6135	UUGGUGUCUCAUUUCUUUUUGGACUAACACGUGGACCAGAGCCGU	0.661	0.662	0.503	0.598
17	6288	CUCUUUGCCUGCAAUUCCUGUGACUGCCAUCAGGUGGCAGAAAAC	0.544	0.474	0.575	0.553
18	6405	UCCAGCCUGGCGACAGAGCAGGACUCUGUCUCAAAAAAAAGAAAG	0.669	0.229	0.63	0.631
19	6480	CCAUCCCUGUUCCUCUUAAAGGACACAAGGGACAUCCACAGGAGG	0.65	0.67	0.664	0.656
20	6489	UUCCUCUUAAAGGACACAAGGGACAUCCACAGGAGGGGAUGACUG	0.643	0.718	0.649	0.649
21	6554	GGAUGUUAGGUAAAAGGAAAGGACAAAUGGCUGGAGAACUGGUGU	0.612	0.264	0.539	0.565
22	6569	GGAAAGGACAAAUGGCUGGAGAACUGGUGUUUCACCCUUCCCUGG	0.603	0.349	0.565	0.575

23	6655	CAGGGUCUGGGCUCCCAGGUGGACCAUGAAACCCUGGCCUGACCA	0.59	0.662	0.636	0.612
24	6731	GGAGCCCCAGUCCCUGACAAGGACCUAGGACAUUUUUGCUCCUGC	0.611	0.675	0.412	0.534
25	6738	CAGUCCCUGACAAGGACCUAGGACAUUUUUGCUCCUGCCCAGCCU	0.653	0.631	0.474	0.58
26	6800	AGCCUUUCAGCUCUGCUGUGUGACUUUGAGGUUGUUGCUCCCCUC	0.489	0.396	0.63	0.541
27	6934	AAGCACAGAAGGGGCAGGAGAGACACUCAGAGGCACUUCCGCUCU	0.531	0.569	0.608	0.564
28	6965	GGCACUUCCGCUCUUGCCCAGGACAUUUUCCCAGCCACACCUUUG	0.657	0.731	0.607	0.641
29	7187	GGGUGCAGCCAGUCGUGUCCGAACUCUCCAAUGACUAAGCGGGGA	0.634	0.612	0.48	0.571
30	7383	AGCGGGGAAGGGGUUCUGAAGAACUCUGGCCAAGAGGACGAGGAU	0.656	0.667	0.387	0.549
31	7696	UAAGAGUCCUGUUGGCUGCAGGACUCAGAGCAUGGACAGGUGGAU	0.668	0.627	0.505	0.601
32	7709	GGCUGCAGGACUCAGAGCAUGGACAGGUGGAUAGUAAAUCACCAC	0.713	0.646	0.622	0.673
33	7739	AUAGUAAAUCACCACCACGGGGACAGCCGUGCCCAGACUGUGCGU	0.575	0.521	0.649	0.602
34	7753	CCACGGGGACAGCCGUGCCCAGACUGUGCGUUUGCUUAGCUCGGG	0.668	0.517	0.549	0.613
35	7777	UGUGCGUUUGCUUAGCUCGGGGACAGCACUUGGCCCGGGGUCUCC	0.559	0.633	0.536	0.554
36	7829	CUCCCUUCAGAGCAUCUGCCAAACUUCGGGCAUCUACCCUGCAAU	0.452	0.436	0.693	0.548
37	7948	GCUGGAGCUGCUUUGCAGAAUGACUUGGGUCUUGCUGGCCCCUGG	0.537	0.701	0.578	0.561
38	8032	UCCCCUUGGUGCCUAACCCAGGACUUUGUCCCCAGAGACCCACUG	0.752	0.786	0.434	0.626
39	8141	AGGCCCAAGGAGGUUGUCAGGGACACACAGCAGGGGGAGGCAGCC	0.666	0.798	0.371	0.554
40	8355	UUGGUCCUUACUCCAUGCCAGGACUUGUGCACAUCUUUUUGGAGC	0.656	0.551	0.48	0.581
41	8786	GCCCAAGGUCACCACCCUCUGAACUGAGGCGUCCCCAACCCAUGC	0.671	0.616	0.429	0.571
42	9344	CGUGACACAAAGAGGGGAGAUGACAGUGGCUGGAGUUGUCAGAGC	0.421	0.368	0.701	0.53
43	9415	AGGCUUGACAGGGCCAAGGGGAACUAUUGUGGAAUGUCUUGGCCU	0.605	0.534	0.61	0.603
44	9736	UGACUCACUCGGGAUCCACUGAACUGGGAGGUCUGUGUCUCCUCC	0.644	0.543	0.528	0.593

45	9807	CCGCAGGAUCACCCAGCUUGGAACUAGAUACAGAAAUGCUGUUUU	0.549	0.601	0.627	0.583

Figures

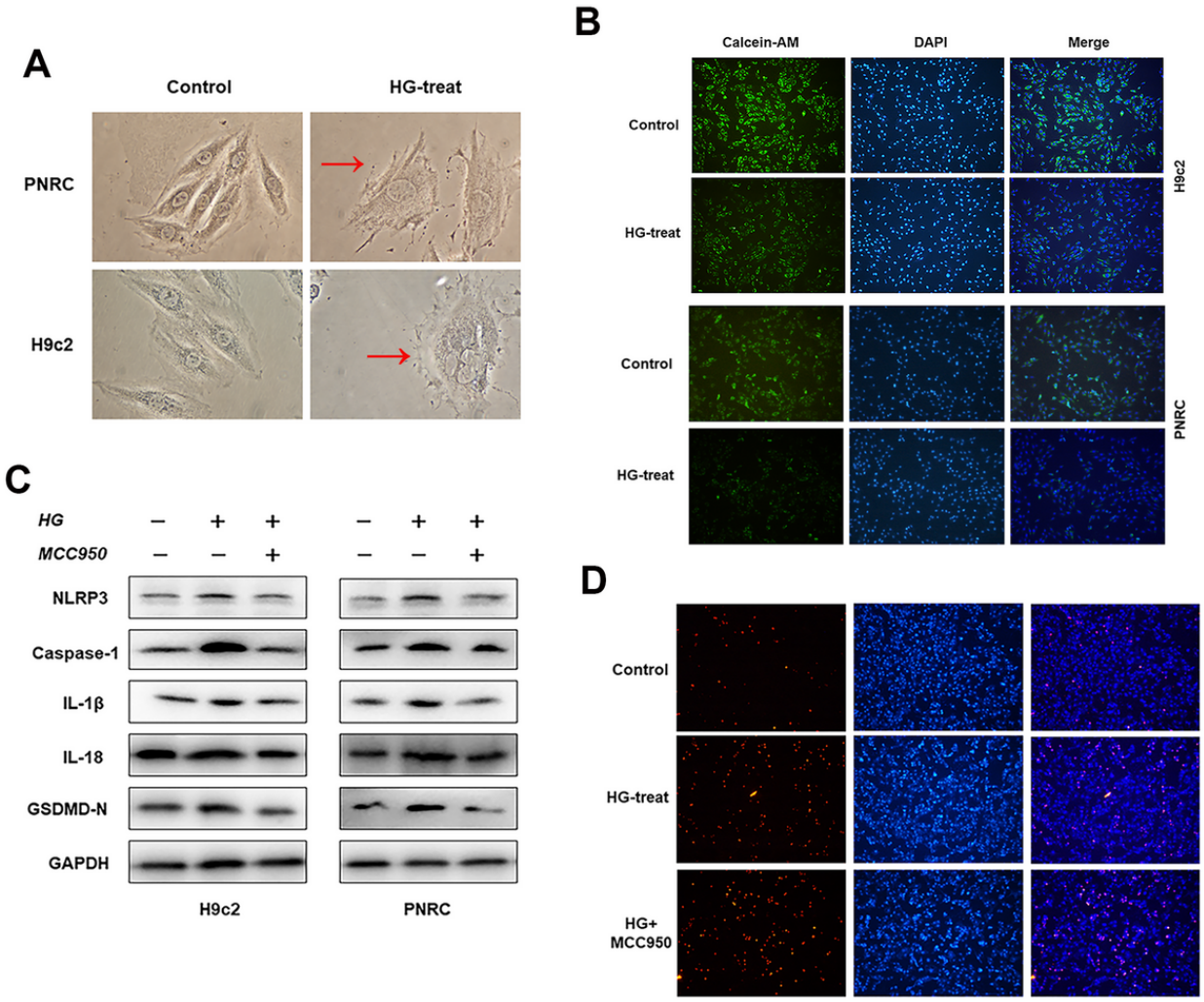

Figure 1

HG treatment induces pyroptosis through targeting NLRP3 A. Morphologic changes of cells cultured with HG were consistent with pyroptosis, including swelling changes and rupture of cell membrane. B. Calcein-AM (dyed with green) staining of HG-treated and controlled cardiomyocytes were shown. C. Western blots were performed to detect the expression level of pyroptosis-related proteins in cardiomyocytes treated with HG or NLRP3 inhibitor MCC950 (5 μg/ml) for 24 h. D. TUNEL staining was used for evaluating the apoptosis level of cardiomyocytes treated with HG and(or) MCC950 (10 mg/kg).

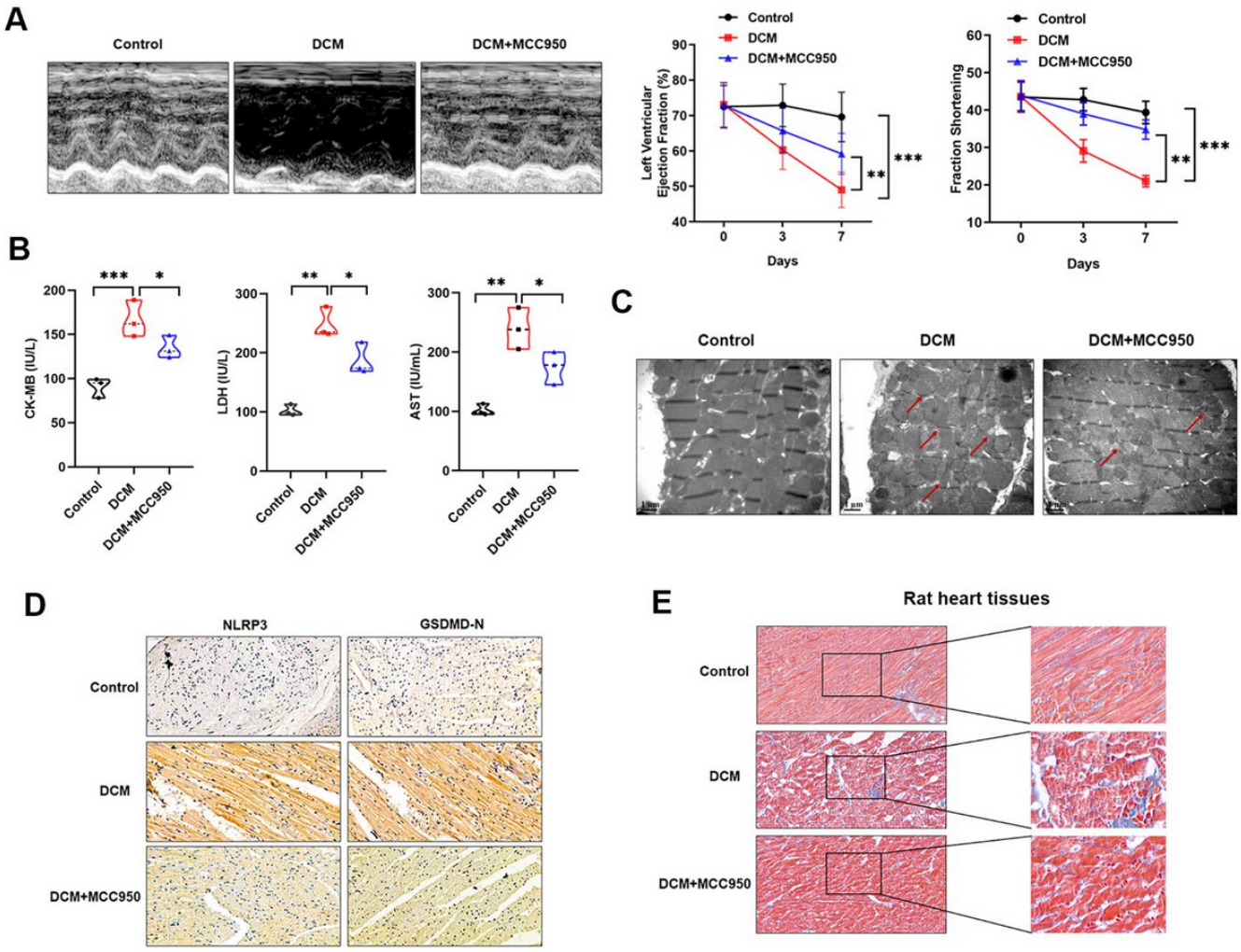

Figure 2

Pyroptosis was involved in DCM in vivo A. Morphological changes (left panel) and quantitative analysis of LVEF and FS (right panel) in rat hearts were detected by echocardiography, **P<0.01, ***P<0.001. B. Serum expression of myocardial enzymes CKMB, LDH and AST were quantified in rats of respective groups, *P<0.05, **P<0.01, ***P<0.001. C. A representative section of the left ventricle from respective groups of rats showing sporadic mitochondrial, damaged disconnected myofibers and thinner myofibers. D. IHC analysis was performed to detect the expression of NLRP3 and GSDMD-N in hearts of DCM rat after treated with MCC950. E. Masson staining was done in heart tissues of DCM rats treated with MCC950.

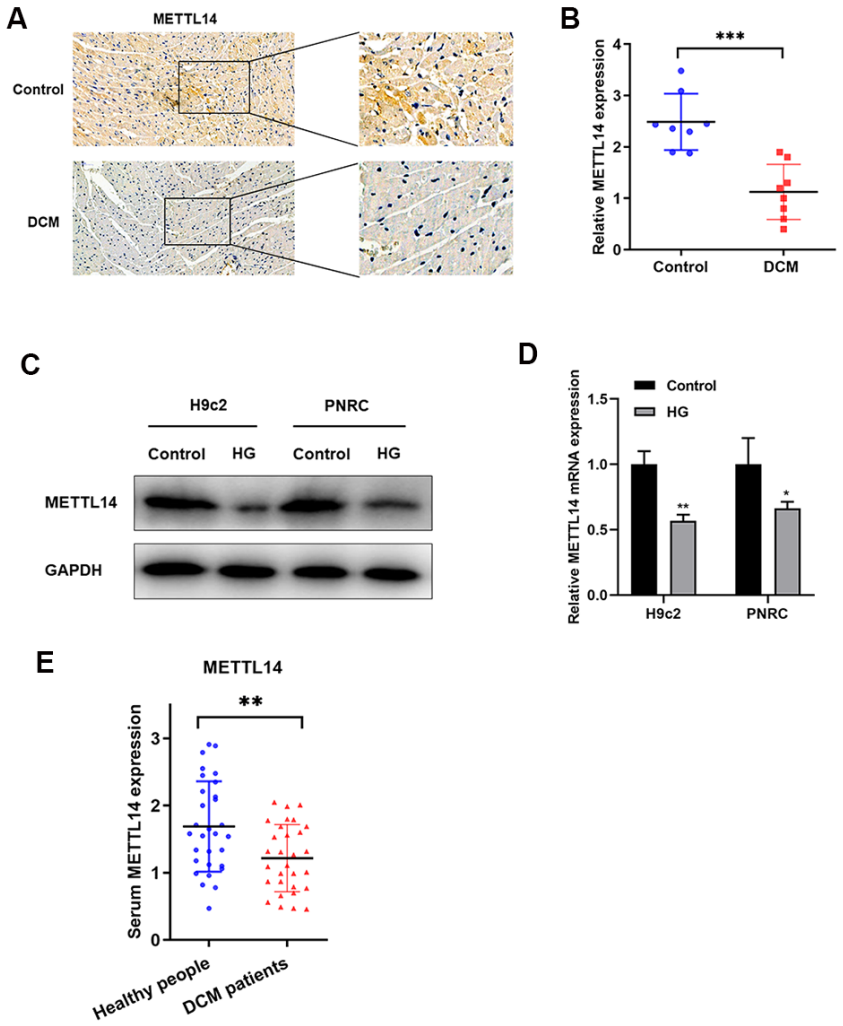

Figure 3

METTL14 was downregulated in DCM rats A. METTL14 protein expression was detected in heart tissues of DCM and control rats. B. Serum circulating METTL14 mRNA was determined in rats of respective groups, ***P<0.001. C-D. METTL14 protein (C) and mRNA (D) levels were detected in cardiomyocytes treated with HG, *P<0.05, **P<0.01. E. Serum METTL14 mRNA was quantified via qRT-PCR in DCM patients and healthy people.

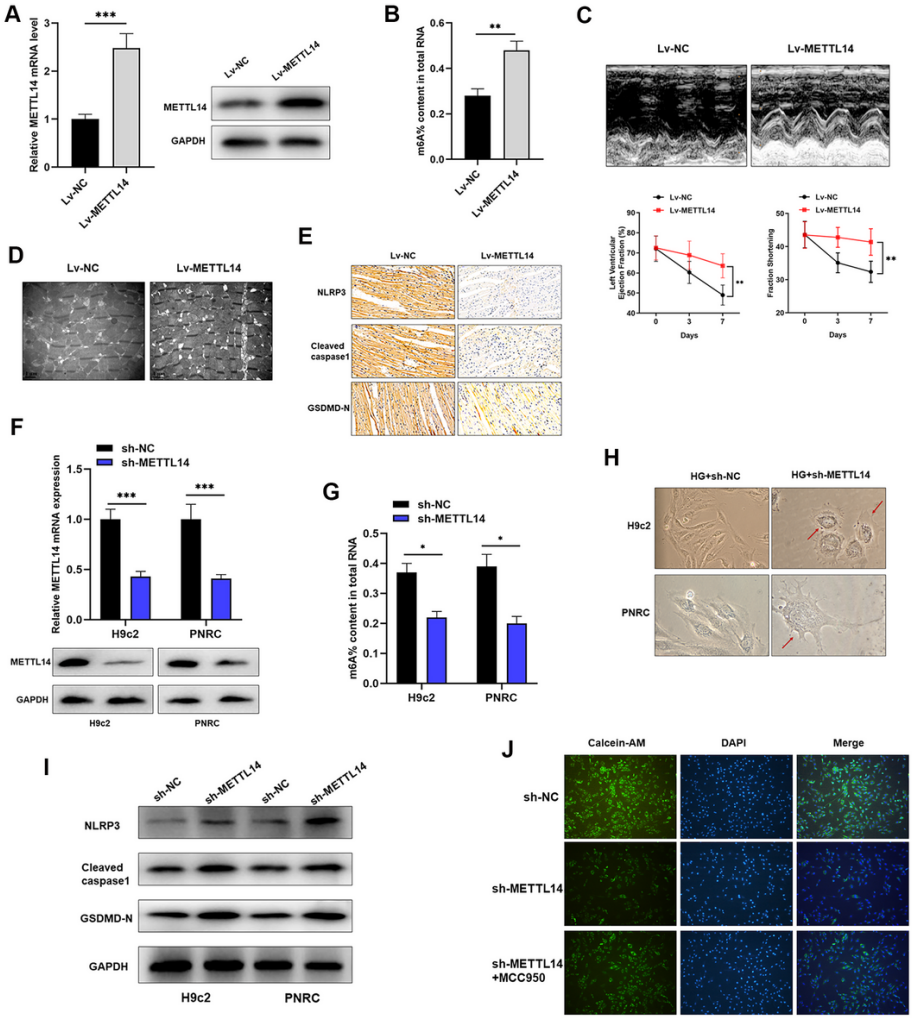

Figure 4

METTL14 suppresses DCM via modulating pyroptosis A. Validation of METTL14 overexpression in DCM rats by western blot and qRT-PCR, ***P<0.001. B. The overall m6A content was increased by upregulation of METTL14, **P<0.01. C. Morphological changes (upper panel) and quantitative analysis of LVEF and FS (lower panel) in rat hearts were detected by echocardiography after injection of METTL14 overexpression vector, **P<0.01. D. Electron microscopy imaging of cardiomyocyte ultrastructure showed that rats overexpressed with METTL14 showed decreased cardiomyocyte damage compared to control group. E. IHC analysis of pyroptosis-related proteins in DCM rats overexpressed METTL14. F. Confirmation of silence of METTL14 in cardiomyocytes at both transcript and protein levels, ***P<0.001. G. knockdown of METTL14 caused significantly downregulated m6A modification level, *P<0.05. H. Morphologic changes of HG-treated cardiomyocytes upon knockdown of METTL14. I. Western blot experiment was carried out to reveal the expression changes of pyroptosis-related proteins in cardiomyocytes transfected with METTL14 silencing vectors. J. Calcein-AM staining showed that deletion of METTL14 increased membrane rupture of cardiomyocytes, however, this effect was reversed by treatment with MCC950.

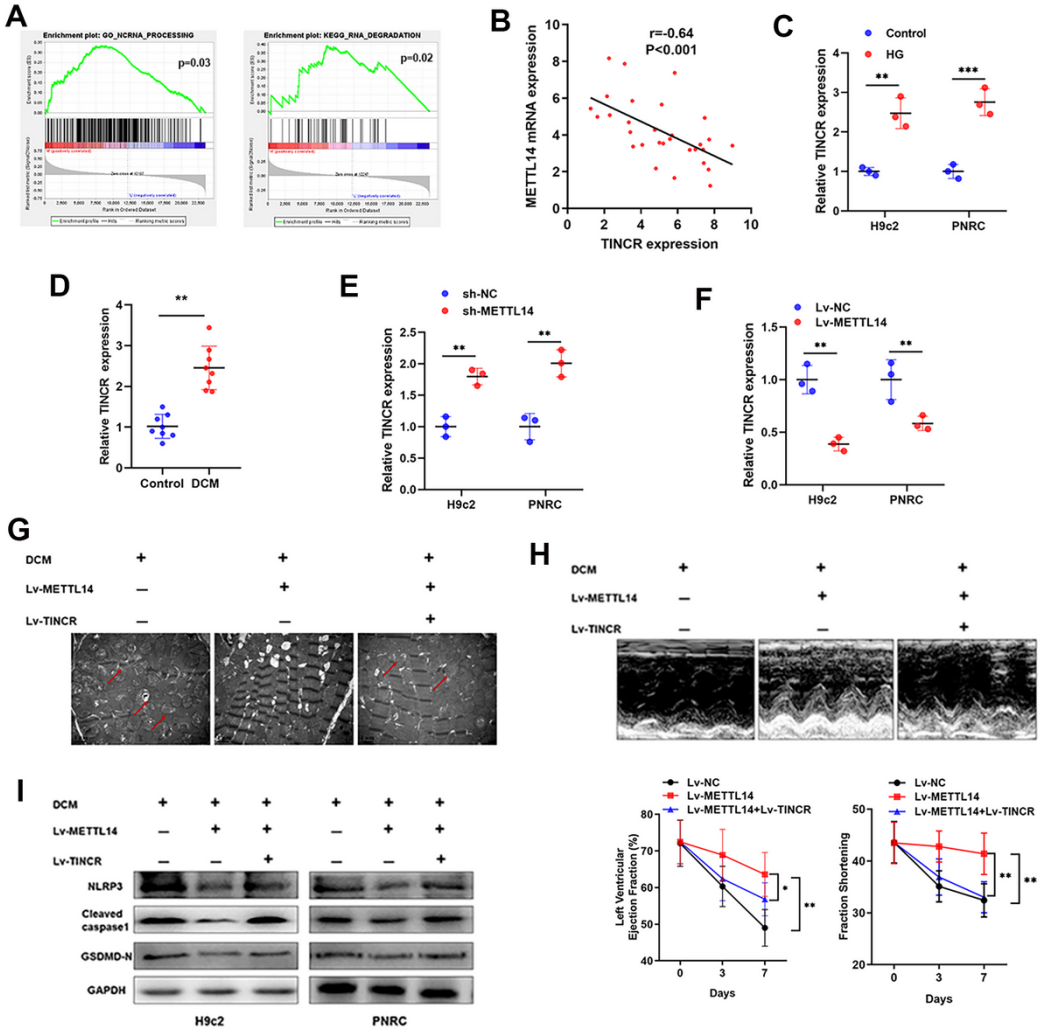

Figure 5

METTL14 suppresses pyroptosis via targeting TINCR lncRNA A. GSEA analysis revealed a positive correlation between METTL14 and ncRNA processing and degradation. B. A significant negative association was identified between METTL14 mRNA and TINCR expression. C. HG treatment of cardiomyocytes significantly increased TINCR expression, **P<0.01, ***P<0.001. D. TINCR was significantly upregulated in DCM rats in contrast to controlled rats, **P<0.01. E-F. qRT-PCR showed that silence of METTL14 (E) upregulated, while overexpression of METTL14 (F) suppressed TINCR expression in cardiomyocytes, **P<0.01. G-I. Cardiac function analysis (G), electron microscopy imaging (H) and western blotting (I) showed that injection of METTL14 dramatically reversed the myocardial damage caused by DCM, however, co-expression of TINCR abrogated the METTL14-mediated influence, *P<0.05, **P<0.01.

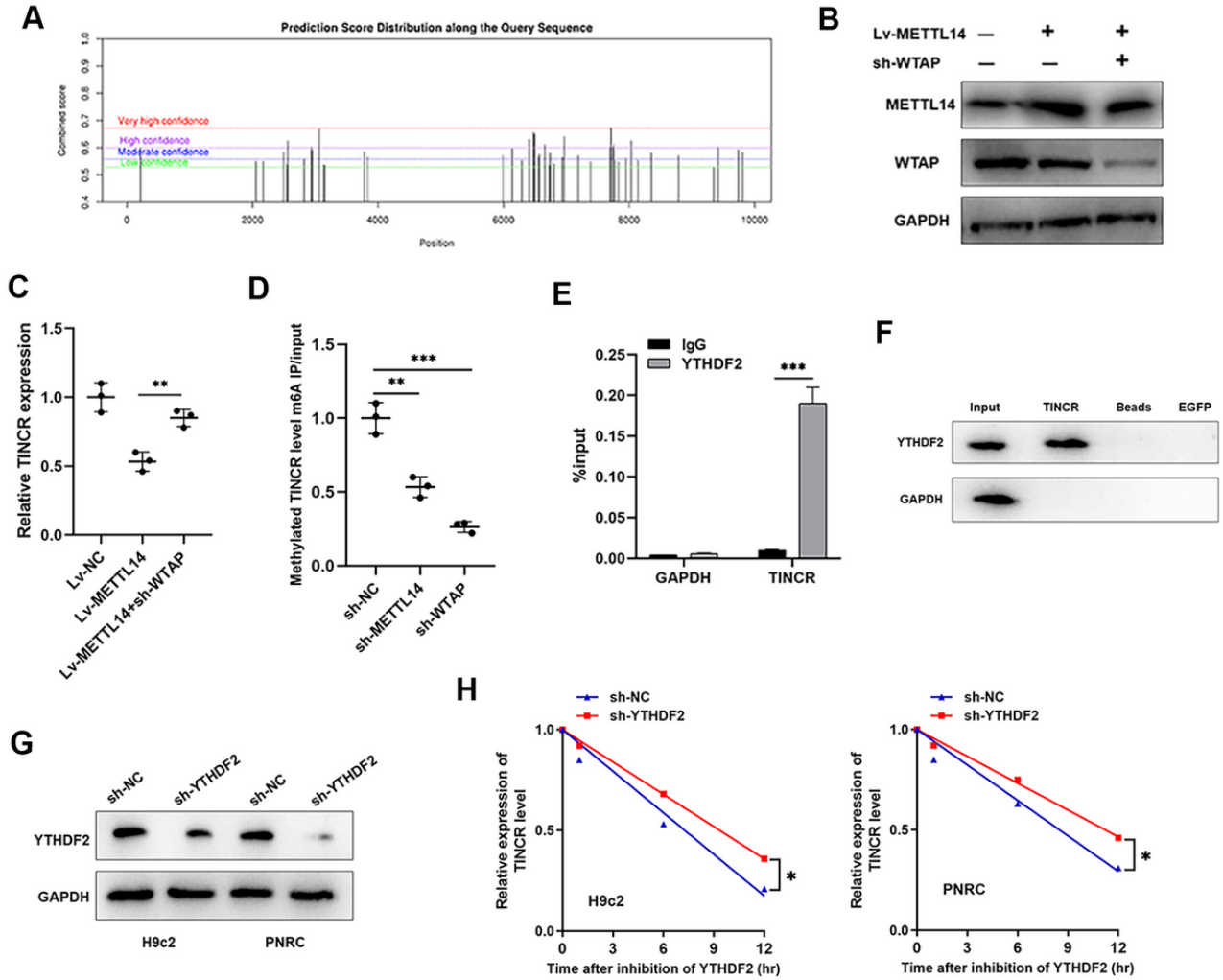

Figure 6

TINCR was downregulated due to the METTL14-mediated m6A methylation A. Predicted binding sites of m6A modification at TINCR sequence according to the online SRAMP database (http://www.cuilab.cn/sramp). B. METTL14-overexpression virus and sh-WTAP vector were injected into DCM rats. Protein band intensity of METTL14 and WTAP were quantified by western blot assay. C. TINCR expression was determined in rats injected with Lv-METTL14 and(or) sh-WATP, **P<0.01. D. Methylated TINCR level was detected via RIP assay, and a significant downregulation by silence of WTAP and METTL14 was observed, **P<0.01, ***P<0.001. E. RIP assay using YTHDF2 antibody revealed a significant association with TINCR, ***P<0.001. F. RNA pulldown experiment showed that YTHDF2 was enriched by TINCR probe. G. Western blot validation of YTHDF2 protein following the transfection of sh-YTHDF2 vector. H. Two cardiomyocyte cell lines were treated with AtcD, then existing TINCR was detected. Silence of YTHDF2 significantly increased degradation of TINCR, *P<0.05.

Image not available with this version

Figure 7

TINCR functions through stabilizing NLRP3 mRNA A. Western blot experiment was performed to test the expression of pyroptosis-related proteins in cardiomyocytes treated with Lv-TINCR and MCC950. B. RNA pulldown using specific TINCR probe revealed a direct interaction between TINCR and NLRP3. C. Cells were treated with ActD, then existing NLRP3 mRNA was detected at different time point. Silence of TINCR significantly decreased NLRP3 stability, P<0.001. D. METTL14 suppressed NLRP3 stability, while co-transfection of Lv-TINCR partially reversed this effect, *P<0.05, **P<0.01. E. A scheme of the proposed mechanisms: TINCR was modified by METTL14-mediated m6A methylation, which induced suppression of TINCR in cardiomyocytes. Suppressed

TINCR caused decreased stability of NLRP3 and thereby induced its downregulation. Eventually, downregulated NLRP3 inhibited pyroptosis and DCM progression.